Picosecond magneto-quantum beats of free excitons in CdS

1998 J. Phys.: Condens. Matter 10 2973

(http://iopscience.iop.org/0953-8984/10/13/014)

J. Phys.: Condens. Matter **10** (1998) 2973–2982. Printed in the UK PII: S0953-8984(98)89063-2

Picosecond magneto-quantum beats of free excitons in CdS

U Müller†, H Stolz‡ and W von der Osten
Fachbereich Physik, Universität-GH Paderborn, Germany

Received 7 November 1997

Abstract. We report the observation of long-lived quantum beats in the 1LO assisted resonance fluorescence of the lowest A exciton in CdS with the twofold spin-degenerate exciton states split by magnetic fields up to 4 T. Excitation by picosecond laser pulses with small spectral width allows us to selectively probe the relaxation dynamics of exciton polaritons at the transverse exciton energy. In this energy region phonon relaxation processes are greatly reduced at low temperatures ($T = 2$ K) leading to the observed long relaxation times of the order of 100 ps. The accuracy of the analysis of the beat signals can be improved by applying the method of linear prediction by singular-value decomposition. This scheme allows us to reveal very weak oscillations and to derive the total exciton splitting due to the magnetic field and due to the strain in the sample.

1. Introduction

Since the first observation of quantum beats for an excitonic transition (Langer *et al* 1990), beat spectroscopy has developed into a well established and useful method to investigate exciton coherence properties. The beating originates from the quantum-mechanical superposition of states which are adjacent in energy and are simultaneously excited by a sufficiently short coherent laser pulse. The period of the beat signal provides the energy state splitting which is usually induced either by magnetic or by strain fields. Equally, from the damping of the beat signal the coherence time τ_{coh} can be determined that is related to the energy relaxation and pure dephasing times T_1 and T_2', respectively by $1/\tau_{coh} = (1/2T_1) + (1/T_2')$ (for details see e.g. Stolz 1994). Besides nonlinear techniques like four-wave mixing (for a recent review see Pantke and Hvam 1994, Phillips 1993 and articles therein), linear time-resolved resonant light scattering, employed in the present study, turned out to be especially successful. Using this method, coherence properties of free excitons in AgBr and Cu_2O as well as of various bound excitons in CdS were studied (Langer *et al* 1990, Stolz *et al* 1991, Langer *et al* 1995).

In this paper we present an investigation of magneto-quantum beats for the $\Gamma_7 \otimes \Gamma_9$ (A) exciton polariton in CdS. This exciton differs from the formerly studied systems in that it has direct character and is electric-dipole allowed while the excitons in AgBr and Cu_2O are indirect electric-dipole allowed and direct quadrupole allowed, respectively. Compared to the recently published study of femtosecond four-wave mixing beats between exciton polaritons derived from different valence bands in CdS (Weber *et al* 1997), the magnetic quantum beats reported here originate from a single exciton-polariton branch.

† Present address: ISAS, Bunsen-Kirchhoff-Strasse 11, D-44139 Dortmund, Germany.
‡ Present address: Fachbereich Physik, Universität Rostock, Universitätsplatz 3, D-18051 Rostock, Germany.

0953-8984/98/132973+10$19.50

As a novel procedure to analyse the beat signals, we use the scheme of linear prediction by singular-value decomposition (LPSVD), a method which was originally introduced to evaluate nuclear magnetic resonance data (Barkhuijsen *et al* 1985). It allows an analysis directly in the time domain and is less sensitive to noise and finite time-windowing effects (leakage) than the discrete Fourier transformation used hitherto. Employing the LPSVD method we were able to uncover several different oscillation frequencies in the measured beat signals. This enabled us to entirely analyse the (transverse) exciton polariton as a function of the external magnetic field, including both singlet and triplet states. In addition to the energies and relevant g-values, the measurements also provide exciton dephasing and energy relaxation times.

2. Experimental details

The investigations were performed by means of a spectroscopic set-up that allows transform-limited measurements and was described in detail elsewhere (Stolz 1994). The optical pulses for excitation were produced by a synchronously pumped tunable dye-laser (Nd:YLF pump; dye: mixture of Stilben 3 and Coumarin 102). They were nearly bandwidth limited with the pulse duration of 5 ps chosen to spectrally cover the splitting of the exciton states ($\approx$400 μeV) produced by applied magnetic fields up to 4 T. Employing a fast photomultiplier (Hamamatsu 2566U) or a streak camera (Hamamatsu C1587) as signal detectors, the overall time resolution was 40 and 18 ps, respectively, with limitations in dynamical range in case of the streak camera.

The sample was grown at the Ioffe Institute, St Petersburg (Russia), by vapour phase sublimation and not intentionally doped. It had cylindrical shape (7 mm in height and 3 mm in diameter) with the crystallographic c-direction along the cylinder axis (figure 1, left). The experiments were performed in Faraday geometry using 180° back-scattering (incident (scattered) light wavevector $\boldsymbol{k}_L$ ($\boldsymbol{k}_s$) parallel (antiparallel) to magnetic field direction $\boldsymbol{B}$). As schematically illustrated in the figure, the c-axis could be rotated by an angle θ up to $\pm 30^\circ$. With the magnetic field applied, this allows for transitions from all exciton states including the triplet states that would not be excited at $\theta = 0^\circ$ due to the selection rules (see figure 1, right, and below).

The beat experiments were performed at $T = 1.\ 8$–2 K.

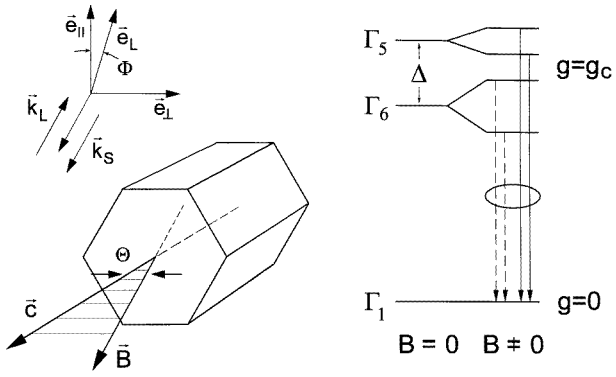

Figure 1. Left: sample and scattering geometry (for explanations see text). Right: free exciton energy levels with and without magnetic field. Transitions shown by dashed lines are only allowed for $\theta \neq 0^\circ$.

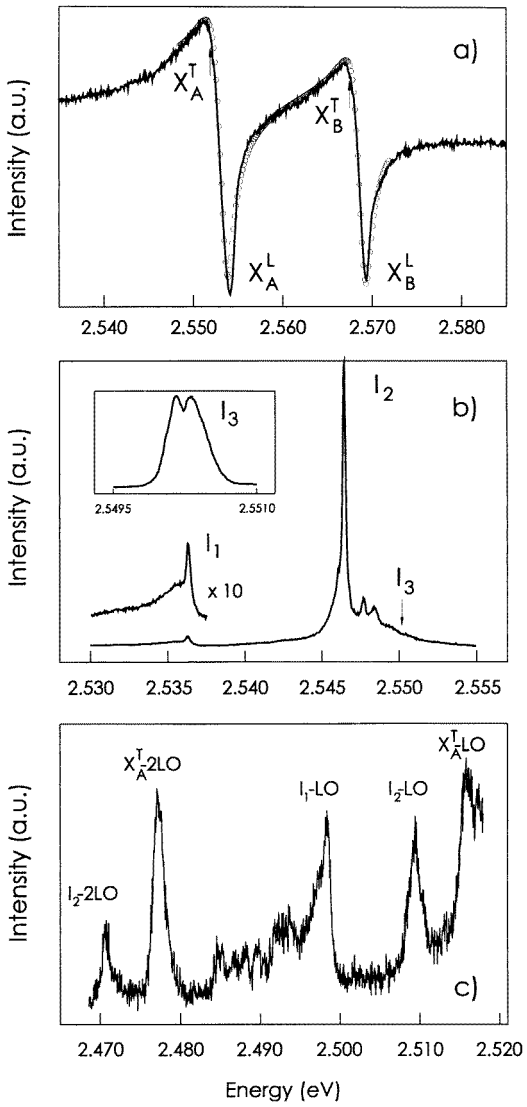

Figure 2. Exciton spectra of the CdS crystal at $T = 1.8$ K. (a) Reflectivity of the longitudinal (L) and transverse (T) components of the A and B exciton polariton. Measured data (full line) are shown with the fit (circles) by a two-oscillator model. (b, c) Bound exciton luminescence excited at $E_L = 2.590$ eV. The inset in (b) shows the laser spectrum tuned to the I_3 absorption that leads to the dip in the laser line intensity.

3. Experimental data

At excitation above the exciton edge, the low-temperature luminescence spectrum of our sample is governed by bound exciton (BX) recombination. As illustrated in figure 2(b), (c), strong I_2 and weaker I_1 transitions along with their 1LO and 2LO replica are observed due to recombination of the exciton at neutral donors (D^0, X) and neutral acceptors (A^0, X), respectively. In addition, tuning the laser spectrum to the absorption of the I_3 line

position reveals the presence of charged donors (D^+, X) which are obviously less efficient recombination centres under non-resonant excitation.

To determine the energy position of the exciton polariton we had to measure the reflectivity spectrum represented in figure 2(a). As expected, it consists of the A, B double structure originating from the valence band splitting into Γ_9 and Γ_7 states (see e.g. Thomas and Hopfield 1962). The energies of the corresponding transverse and longitudinal exciton components (X^T, X^L) were obtained by fitting a standard two-oscillator model to the experimental data (Hopfield 1958). In the quantum beat measurements, the excitation was accomplished in resonance with the X_A^T ($n = 1$) exciton polariton at energy 2.5521 eV. The scattered light was detected at the 1LO replica in order to avoid any disturbing effect of the elastically scattered light at the exciting laser frequency.

Figure 3 displays the light scattering signal as a function of time observed with and without magnetic field after pulsed excitation. The exciting laser was linearly polarized (polarization vector $\boldsymbol{e}_L$ in figure 1) with $\phi = 0^\circ$. The scattered light was analysed with linear polarizations $\boldsymbol{e}_S \parallel \boldsymbol{e}_L$ and $\boldsymbol{e}_S \perp \boldsymbol{e}_L$ giving corresponding intensities $I_\parallel$ and $I_\perp$. According to the theory of light scattering (for details see Stolz 1994), at zero magnetic field $I_\parallel$ represents the coherently scattered (Raman) part of the emitted signal while the depolarized component $I_\perp$ is luminescence-like. As anticipated, these signals differ in time behaviour, the small depolarized intensity demonstrating that the pure dephasing by elastic

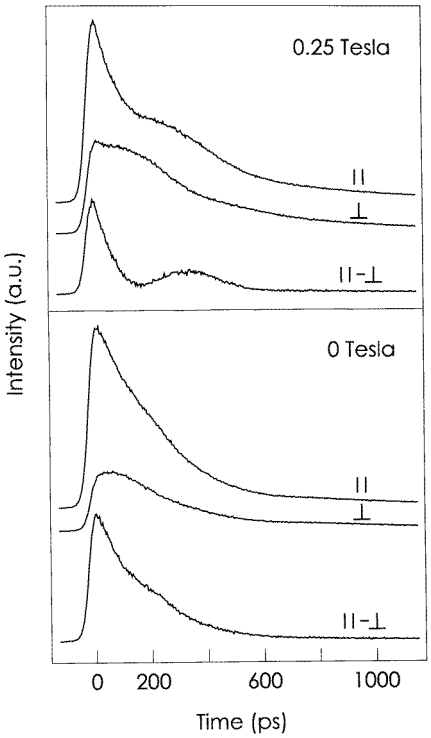

Figure 3. Time dependence of the scattered intensity observed after pulsed excitation at the X_A^T resonance and detected in the X_A^T–1LO replica in zero magnetic field and for $B = 0.25$ T, $\theta = 5^\circ$. Photomultiplier measurement with time resolution 40 ps. Excitation with linearly polarized light ($\phi = 0^\circ$). The scattered light is linearly polarized with $\phi = 0^\circ$ ($I_\parallel$) and $\phi = 90^\circ$ ($I_\perp$), respectively. The intensity difference $I_\parallel - I_\perp$ represents the coherently scattered intensity.

scattering is apparently weak. With the magnetic field applied, clear beating is observed in both polarizations. In these data, the amplitude ratio of the oscillating part and the background is a direct measure of the (relative) contributions of coherent and incoherent scattering. Also plotted is the intensity difference $I_{\parallel} - I_{\perp}$. In the so-called 'white-light limit', i.e. in the case of broad-band excitation and detection that is approximately realized in our experiments, this quantity represents the coherent contribution to the light scattering.

As schematically shown in figure 1, the free exciton has a Γ_1 ground state and excited states with symmetries Γ_5 (optically dipole allowed) and Γ_6 (dipole forbidden), twofold degenerate each and separated by the electron–hole exchange energy Δ (Thomas and Hopfield 1962). The magnetic field removes this degeneracy. In figure 3, the oscillatory structure essentially originates from the split Γ_5 state, with the low-frequency oscillation that is visible at $B = 0$ T revealing the presence of a small zero-field strain splitting.

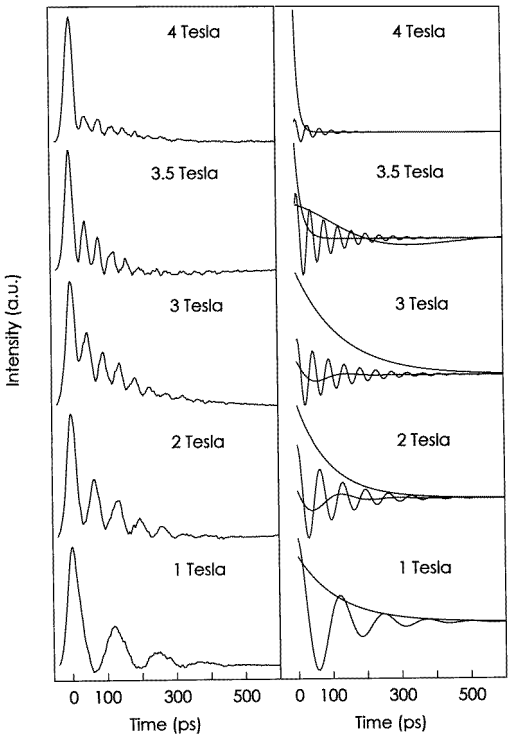

Figure 4. Time dependence of the coherent part of the intensity $I_{\parallel} - I_{\perp}$ at different magnetic fields. Left: streak camera measurements with time resolution 18 ps. Right: decomposition by the LPSVD method into various decay curves as described in the text.

Figure 4 (left) displays a series of time-dependent data $I_{\parallel} - I_{\perp}$ taken with the streak camera. Compared with the data in figure 3, the time resolution here is improved by more than a factor of two. This enables one to resolve higher frequencies and, hence, measure larger energy splittings. Still more important, from inspecting the plots in detail it becomes quite evident that at certain field strengths more than only one oscillation period must be contained in the measured signal. It suggests that the laser pulse excitation, apart from causing the superposition of the predominant singlet states, also produces interferences with the weakly allowed triplet states. Because the angle between the crystal c-axis and the

magnetic field in the experiment was chosen as $\theta = 5^\circ$, transitions from the Γ_6 triplet states become allowed rendering possible quantum interferences involving all four exciton states.

4. Method for analysis

Quantum beat signals in the 'white-light limit' consist of a series of exponentially damped sinusoids (Stolz 1994). The oscillation frequencies and amplitudes are determined by the energy splittings and the transition moments of the excited levels, respectively. The standard procedure that has been used so far to analyse such a signal is to Fourier transform the data and perform a fit of the line positions and half-widths in the resulting spectrum. This method, however, has several drawbacks as the number of lines to be fitted is *a priori* unknown and can be inferred from the spectrum only with a certain ambiguity.

In order to analyse the present data we employed the LPSVD method (linear prediction by singular-value decomposition) developed in the area of nuclear resonance (Barkhuijsen *et al* 1985). It allow us, in the time domain, to fit a finite number of superimposed exponentially damped trigonometric functions having arbitrary phases and exhibiting noise. More specifically all frequencies, amplitudes, damping constants and phases inherent in the measured time dependent signal can be determined thus providing the exciton state splittings and coherence times.

One starts off with the assumption that the measured data points x_n ($n = 1, \ldots, N$) can be expressed as a sum of K exponentially damped trigonometric functions

$$x_n = \sum_{k=1}^{K} c_k \exp(-d_k n \Delta t) \cos(\omega_k n \Delta t + \varphi_k) + R_n \tag{1}$$

with ω_k, d_k, c_k and φ_k denoting the frequencies, damping constants, amplitudes and phaseshifts. Δt is the sampling interval. R_n represents the noise in the measured points. Then one sets up N–M linear equations that express each of the first N–M data points as a linear combination of the following M data points written as

$$\boldsymbol{x} = \mathbf{X}\boldsymbol{a} \tag{2}$$

where $X_{k,i} = x_{k+i+1}$ (with $k = 1, \ldots, N$–M, $i = 1, \ldots, M$) is the N–$M \times M$ backward prediction matrix, $\boldsymbol{x}$ is the vector of the first N–M data points and $\boldsymbol{a}$ the unknown vector of linear prediction coefficients.

If the noise in the signal is zero ($R_n = 0$) it can be shown (Lawson and Hanson 1974) that the unique solution of (2) is given by

$$\boldsymbol{a} = \mathbf{V}\mathbf{L}^T\mathbf{U}^T\boldsymbol{x} \tag{3}$$

with $\mathbf{U}$, $\mathbf{V}$, $\mathbf{L}$ denoting the singular-value decomposition $\mathbf{X} = \mathbf{U}\mathbf{L}\mathbf{V}^T$. $\mathbf{L}$ is a diagonal N–$M \times M$ matrix, the rank l of which is given by $l = 2K$ and exactly $M = 2K$ prediction coefficients are needed. From the LP coefficients a_i (with $i = 1, \ldots, M$) the frequencies ω_k and damping constants d_k ($k = 1, \ldots, K$) of the sinusoids are given by the roots r_k of the polynomial of order M

$$z^M - a_1 z^{M-1} - \cdots - a_M = 0 \tag{4}$$

as

$$\exp[(d_k \pm \mathrm{i}\omega_k)\Delta t] = r_k. \tag{5}$$

(5) shows that a root is either real and corresponds to a simple exponential with $\omega_k = 0$, or two roots are the complex conjugate of each other and thus determine a single oscillation.

In the case of a *noisy measurement*, the number of prediction coefficients should be chosen much larger than the expected number of exponentials (usually the procedure works best with $M = 0.5N, \ldots, 0.75N$). (3) is now the optimal solution in the sense of minimizing the least-squares error with regard to the experimental data. The diagonal elements of $\mathbf{L}$, the singular values λ_i ($i = 1, \ldots, M$), are now in general all non-zero. If the noise is not too excessive, however, the singular values that correspond to significantly contributing sinusoids are much larger than those connected to the noise in the data (see figure 5(a)). Therefore in most cases the number of significant exponentials can be readily determined (here we set $l = 5$). Furthermore, the stability of the algorithm can be increased considerably by setting all noise related LP coefficients ($i > 2K$) to zero. As can be seen from (5), the significant roots of the polynomial (4) all lie outside the unit circle in the complex plane (see figure 5(b), where the real and imaginary parts of all the roots are plotted in the complex plane) allowing a further check of the analysis (here obviously $K = 3$). Once the frequencies and damping constants are determined, the amplitudes and phases can be found by a second least-squares procedure from the measured data.

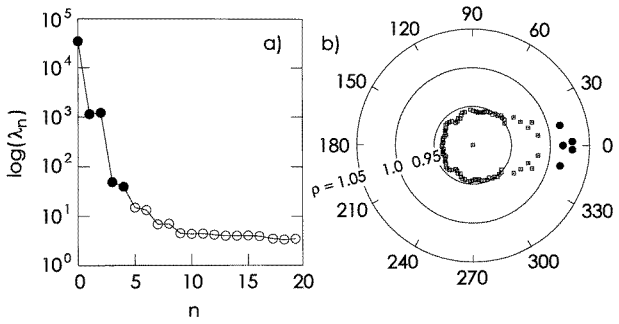

Figure 5. (a) Singular values λ_n of the SVD decomposition of the 3 tesla measurement in figure 4 displayed on a logarithmic scale. The full dots represent those singular values that are meaningful damped oscillations of the signal. (b) Roots of the polynomial of the SVD analysis in a complex polar plot. The real and imaginary parts represent the damping constant and the oscillation frequency of the damped sinusoids, respectively (see text). ρ denotes the circle radius.

Employing this procedure, we have decomposed the measured data as shown on the right-hand side in figure 4. The dominant oscillatory signal, decreasing in amplitude at higher fields, is ascribed to the superposition of the singlet states. At intermediate field strengths (2–3.5 T), an additional lower-frequency signal is uncovered with an amplitude that varies with field strength. We ascribe this component to the interference of exciton singlet states and the weakly allowed triplet states. Finally, as already evident from the shape of the experimental curves, an exponentially decaying signal is found which has appreciable amplitudes and varies in decay time depending on field strength (see below).

5. Results and discussion

Evaluating the oscillation periods, in figure 6 (top) the energy splittings are plotted against magnetic field strength (full and open circles). To fit these data, we have calculated the magnetic field dependence of the exciton states (figure 6, below) by numerical diagonalization of the total Hamiltonian

$$H_{total} = g_e \mu_B \boldsymbol{B} \cdot \boldsymbol{s} - g_v^{\parallel} B_z \sigma_z + H_{strain}. \tag{6}$$

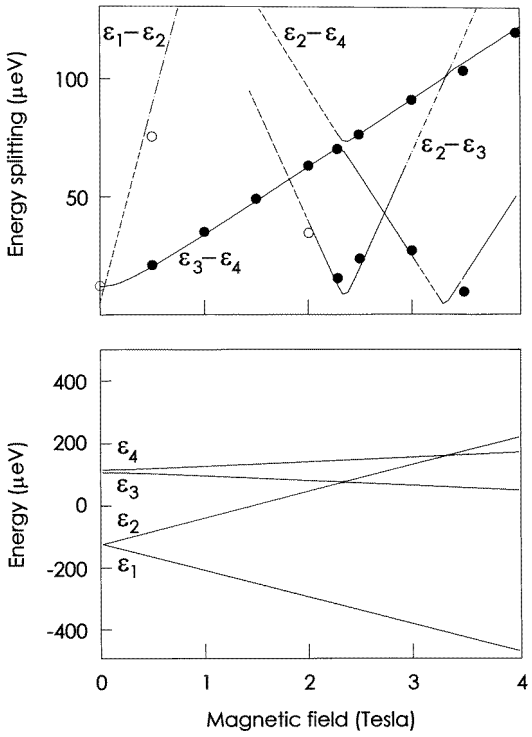

Figure 6. Top: energy splittings of the free exciton states as function of magnetic field strength. The points represent experimental data with energy values derived from weaker signals due to triplet states indicated by open circles, the full (strong signals) and dashed (weak signals) lines are the calculated energy splittings from the curves in the lower figure. Below: energy singular values calculated from (1) and (2) with the parameters given in the text. $\varepsilon_{1,2}$ and $\varepsilon_{3,4}$ denote triplet and singlet state energies, respectively.

As has been discussed in detail in a previous study of donor-bound excitons (Stolz *et al* 1991), besides the electron and hole Zeeman terms, H_{total} comprises a strain term. It accounts for the strain-dependent exchange splitting and is given by

$$H_{strain} = 2\Delta s_z\sigma_z + C_1[(\varepsilon_{xx} - \varepsilon_{yy})s_x\sigma_x - 2\varepsilon_{xy}s_y\sigma_x] + C_2[(\varepsilon_{xx} - \varepsilon_{yy})s_y\sigma_y + 2\varepsilon_{xy}s_x\sigma_y] + C_3[\varepsilon_{xz}s_x\sigma_z + \varepsilon_{yz}s_y\sigma_z]. \quad (7)$$

s_x, s_y, s_z, σ_z are corresponding components of the effective electron and hole spin operators ($s = \sigma = \frac{1}{2}$, z-axis $\|$ crystallographic c-axis). Δ, $\varepsilon_{\alpha,\beta}$ and C_i are the exchange energy at zero strain, the strain tensor components and appropriate deformation potential constants that, together with the electron and hole g-factors (g_c, $g_v^{\|}$ in (1)), serve as fitting parameters. Calculating the exciton energies, the best fit to the measured data in figure 6 (top) is obtained using the following values:

$$g_c = 1.75$$
$$g_v^{\|} = 1.23$$
$$\Delta = 0.235 \text{ meV}.$$

These values are in good agreement with previously published data (Landolt–Börnstein 1983). In addition, our sample exhibits strain along the x-direction and in the xz-plane

resulting in zero-field splittings $C_1\varepsilon_{xx} = 4$ μeV and $C_3\varepsilon_{xz} = 3$ μeV. The strengths of the various transitions are obtained straightforwardly by the diagonalization of the total Hamiltonian as singlet-state mixing coefficients.

Without strain, the exciton transitions from the Γ_5 and Γ_6 states (see figure 1, right) are left and right circularly polarized. The existing strain splitting at $B = 0$ T, however, results in linear polarizations transforming into elliptically and circularly polarized light at intermediate and high B-field strengths (Zeeman splitting $\gg$ strain splitting). Since the scattered light is analysed by a linear polarizer along orthogonal directions ($\boldsymbol{e}_\parallel$, $\boldsymbol{e}_\perp$ in figure 1), this results in an intensity background explaining the exponentially decaying contribution in figure 4.

As to the determination of the coherence and energy relaxation times we have found a considerable dependence upon the sample spot. Even though a CCD camera was used to select or control a certain position of the excitation beam at the sample, in different experiments τ_{coh} varied between 90 and 210 ps while T_1 was found between 140 and 370 ps. We believe these variations are extrinsic in origin although the exact nature is not yet clear. As we were able to find beating of the X_A^T exciton states only in selected samples, the structural and surface quality and the impurity content are considered as important factors.

To make sure that phonon assistance in the exciton decay does not affect the coherence time, we have also detected the beat signal at the X_A^T–2LO replica (figure 2(c)) thereby trying not to change the sample spot. Comparing with the 1LO replica results, the beat frequency and τ_{coh} agree well within the accuracy of the analysis demonstrating that the same spot at the sample was investigated. However, we found that the energy relaxation time T_1 was longer by a factor of 2 suggesting additional incoherent hot luminescence processes contribute to the emission.

In the analysis we have neglected the polariton character of the A exciton states. This is justified because the beats were observed under excitation conditions where only exciton-polariton states from the lower branch around the bottle-neck region are excited. In this context it is interesting to compare the coherence times τ_{coh} obtained by our method to the results of a recently published four-wave mixing study (Weber *et al* 1997). In this paper, quantum beats between the A and B exciton-polariton states are observed after excitation by femtosecond laser pulses. As compared with our results the dephasing times (corresponding to $2\tau_{coh}$) were found to be two orders of magnitude smaller. This is conceivable in view of the much larger spectral bandwidth of the femtosecond pulses which excite polaritons that have a wide range of wavevectors and, hence, can be expected to have very different relaxation behaviour and times. In contrast, in the present case of picosecond pulses with small spectral width, only a single state is excited and its relaxation measured.

6. Concluding remarks

Besides at the free exciton polariton, we have searched for quantum beating at the donor and acceptor BX transitions (figure 2). Using resonant excitation and detection in the LO phonon replica as before, for the neutral acceptor and donor BX (transitions I_1 and I_2) we could not detect any beating. At zero $\boldsymbol{B}$-field, with appropriate polarizations of the incident and scattered light (σ^+ and σ^+, σ^-, respectively; see e.g. Bonnot *et al* 1974) rapid depolarization is observed suggesting short coherence times. We therefore believe that the lack of beating structure is caused by insufficient time resolution rather than by complications due to the degeneracy of the (A^0, X) and (D^0, X) ground states. These states have symmetries Γ_9 and Γ_7, respectively, but will be split by the magnetic field. Still, based on symmetry and under the experimental conditions chosen ($B > 1$ T, $\theta = 30^\circ$), one would

expect beating between pairs of transitions that start from the two excited state sublevels and end in a common final state which is a prerequisite for beating to occur.

In contrast, pronounced beating was found for the I_3–1LO luminescence line (D^+, X) and allowed a detailed analysis along the lines reported earlier (Stolz *et al* 1991). Different from these previous measurements, the coherent part of the scattering ($I_\parallel - I_\perp$) showed an additional exponentially decaying intensity component as observed for the free exciton (X_A^T). As the selection rules for the I_3 line are identical with those for the free exciton, this contribution can be explained by the combined effect of strain and magnetic field as in the case of the free exciton (see section 5 above).

Acknowledgments

The authors are indebted to Professor S Permogorov, St Petersburg (Russia), for providing samples. They also appreciate the support of the project by the Deutsche Forschungsgemeinschaft.

References

Barkhuijsen H, de Beer R, Bovée W M M J and van Ormondt D 1985 *J. Magn. Res.* **61** 465
Bonnot A, Planel R and Bénoit à la Guillaume C 1974 *Phys. Rev.* B **9** 690
Göbel E O, Koch M, Feldmann J, von Plessen G, Meier T, Schulze A, Thomas P, Schmitt-Rink S, Köhler K and Ploog K 1992 *Phys. Status Solidi* b **173** 21
Hopfield J J 1958 *Phys. Rev.* **112** 1555
Landolt–Börnstein New Series 1983 vol 17b (Berlin: Springer)
Langer V, Stolz H and von der Osten W 1990 *Phys. Rev. Lett.* **64** 854
——1995 *Phys. Rev.* B **51** 2103
Lawson C L and Hanson R J 1974 *Solving Least Squares Problems* (Englewood Cliffs, NJ: Prentice-Hall)
Pantke K-H and Hvam J M 1994 *Int. J. Mod. Phys.* B **8** 73
Phillips R T (ed) 1993 *Coherent Optical Interactions in Semiconductors (NATO ASI Series B: Physics 330)* (New York: Plenum)
Stolz H 1994 *Time Resolved Light Scattering from Excitons (Springer Tracts of Modern Physics 130)* ed R D Peccei, F Steiner, J Trumps and P Wölfe (Berlin: Springer) p 85
Stolz H, Langer V, Schreiber E, Permogorov S and von der Osten W 1991 *Phys. Rev. Lett.* **67** 679
Thomas D G and Hopfield J J 1962 *Phys. Rev.* **128** 2135
Weber D, Petri W, Woggon W, Klingshirn C F, Shevel S, and Göbel E O 1997 *Phys. Rev.* B **55** 12 848